I&EC research
Industrial & Engineering Chemistry Research

Article

pubs.acs.org/IECR

Inert Carbon Nanoparticles for the Assessment of Preferential Flow in Saturated Dual-Permeability Porous Media

Chuanjin Yao,*[,†,§,∥,#] Yushi Zhao,[‡,§,#] Guanglun Lei,[†] Tammo S. Steenhuis,[∥] and Lawrence M. Cathles*[,‡,§]

[†]School of Petroleum Engineering, China University of Petroleum (East China), Qingdao, Shandong 266580, China
[‡]Department of Earth and Atmospheric Science, Cornell University, Ithaca, New York 14853, United States
[§]KAUST−Cornell Center for Energy and Sustainability, Cornell University, Ithaca, New York 14853, United States
[∥]Department of Biological and Environmental Engineering, Cornell University, Ithaca, New York 14853, United States

ABSTRACT: Knowledge of preferential flow in heterogeneous environments is essential for enhanced hydrocarbon recovery, geothermal energy extraction, and successful sequestration of chemical waste and carbon dioxide. Dual tracer tests using nanoparticles with a chemical tracer could indicate the preferential flow. A dual-permeability model with a high permeable core channel surrounded by a low permeable annulus was constructed and used to determine the viability of an inert carbon nanoparticle tracer for this application. A series of column experiments were conducted to demonstrate how this nanoparticle tracer can be used to implement the dual tracer tests in heterogeneous environments. The results indicate that, with the injection rate selected and controlled appropriately, nanoparticles together with a chemical tracer can assess the preferential flow in heterogeneous environments. The results also implement the dual tracer tests in heterogeneous environments by simultaneously injecting chemical and nanoparticle tracers.

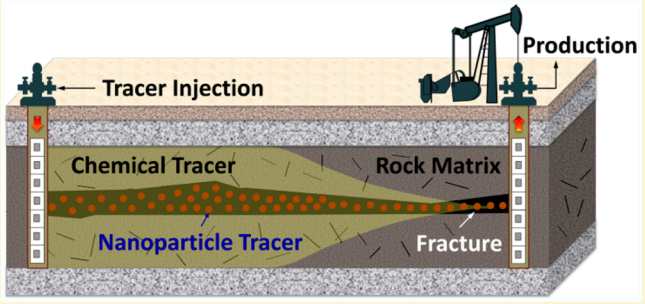

1. INTRODUCTION

Fluid flow in structured soils, fractured aquifers, geothermal fields, and hydrocarbon reservoirs often has a dual character: part of the fluid is mobile and flows along the connected porosity, fractures, or channels, while another part remains immobile or stagnant within the structural units.[1] Exchange of fluid and solutes between the two parts may occur through diffusion.[2,3] One aspect, which is of great importance in enhanced hydrocarbon production or chemical waste and carbon dioxide sequestration in depleted hydrocarbon reservoirs, is the ability of the displacement fluids, chemical contaminants, inorganic solutes, or carbon dioxide to diffuse from the fractures or channels into the surrounding matrix that still contains a large amount of stagnant hydrocarbons.[4−6] Making flow more uniform will result in enhanced hydrocarbon recovery, extract geothermal energy more effectively, and increase the effectiveness of chemical waste and carbon dioxide sequestration.[7,8]

Nanoparticle tracers have long been seen as an effective way to assess the uniformity of fracture-controlled or channelized flow and the effectiveness of diffusion within the surrounding matrix.[9−11] It has been long recognized that nanoparticle tracers could travel obviously faster than conventional chemical tracers because they diffuse much less from the fractures or channels into the surrounding matrix.[12] Chemical tracers, in contrast, could diffuse rapidly enough from the fractures or channels into the surrounding matrix to directly indicate the total porosity. Therefore, comparing the arrival behavior of nanoparticle and chemical tracers would indicate the degree of preferential flow, as illustrated in Figure 1. Cathles et al.

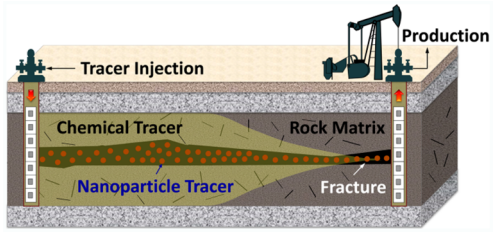

Figure 1. Concept of dual chemical−nanoparticle tracer method.

conducted the first tests of this idea, but the method proved to be problematic.[13] Many previous attempts to use nanoparticles as tracers have failed largely because these nanoparticles stick or are retained.[14,15]

With respect to this dual-tracer methodology, the nanoparticles should be in appropriate particle size, should also be

Received: January 15, 2017
Revised: May 4, 2017
Accepted: June 7, 2017
Published: June 7, 2017

DOI: 10.1021/acs.iecr.7b00194
Ind. Eng. Chem. Res. 2017, 56, 7365−7374

stable in subsurface conditions, and should be detectable at parts per million concentrations.[6] In this paper, we introduced inert carbon nanoparticles of 2−5 nm in diameter. They are much larger than molecules (0.1−1 nm) but smaller than all but the very smallest subsurface pores. They have aqueous diffusion coefficients 1−1.5 orders of magnitude less than chemical tracers whose aqueous diffusion coefficients can be directly measured through the method reported by Newman.[16] They are small enough to path through the fractures or channels and can form stable dispersions in aqueous solutions. What is more important is that the nanoparticles are almost inert and do not stick on rock surfaces and minerals.[17,18] Few studies have focused on their transport in porous media with fractures or channels. Little is known about how these nanoparticles implement the dual tracer tests in physically heterogeneous environments.

Most research to assess the preferential flow in heterogeneous environments often involve traditional two parallel columns, one of which is more permeable than another, and measure the fractional flow rates in each column.[19−21] Although the fractional flow curves from these column experiments can provide valuable insights into the preferred flow, this configuration does not address mass exchange between permeable and impermeable zones[22] and could lead to an invalid interpretation. In structured heterogeneous columns with tubules embedded in the matrix of sand, the factors controlling the migration of colloidal particles can be better understood, but these columns do not accurately reflect the advection−diffusion characteristics of actual heterogeneous environments.[23]

In this work, we constructed a saturated dual-permeability model with a variable diameter copper screen tube that separated coarse sand from fine sand to avoid the problems of the present heterogeneous columns. The breakthrough curves were used to analyze the arrival behavior of nanoparticle and chemical tracers. Thus, the aim of this research is to determine the viability of an inert carbon nanoparticle tracer for the assessment of preferential flow in heterogeneous porous media, and to demonstrate how this nanoparticle tracer can be used to implement the dual tracer tests in actual heterogeneous environments.

2. EXPERIMENTAL SECTION

2.1. Dual-Permeability Model. The model with an interior chamber of 17.50 cm length and 1.95 cm diameter was constructed from a clear acrylic tube. As illustrated in Figure 2, this model consists of fittings that connect to the influent and effluent tubing, copper filters to contain the sand, rubber O-ring seals, an acrylic tube of 17.50 cm in length and 1.95 cm in internal diameter, and a variable diameter copper screen tube that separates coarse sand in the central core from fine sand in the annulus. This model is a dual-permeability model with a high permeable core surrounded by a low permeable annulus, and can reflect the dual character of fluid flow in solid rocks and structured soils. Besides, this model is convenient to clean and can be packed with sand repeatedly.

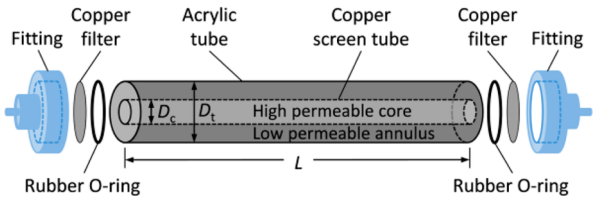

Figure 2. Diagram of dual-permeability model. The copper screen tube was removed when packing the homogeneous columns.

2.2. Materials and Reagents. The nanoparticle tracer used in our experiments consists of carbon-cored fluorescence nanoparticles (abbreviated Cdot) that were synthesized in a one-step thermal decomposition of citric acid monohydrate and ethanolamine in a 1−3 molar ratio and functionalized with highly hydrophilic polymer corona hairs, as described by Krysmann et al. and Markova et al.[24,25] The size of these nanoparticles dispersed in aqueous solution is 2−5 nm in diameter, and the zeta potential at pH 7 is −5 mV, as determined with a Zetasizer Nano system (Malvern Instrument Ltd., Malvern, U.K.). Their intense fluorescent emission allows them to be easily detected at low concentrations of approximately 0.01 ppm using a spectrofluorimeter. For comparison, bromide (in the form of KBr) was chosen as a conventional chemical tracer because it is small, is diffusive, and can be detected at low concentrations. With respect to nanoparticles in the 2−5 nm diameter range, the aqueous diffusion coefficients, calculated using the Stokes−Einstein equation,[16] are in the range 2.1×10^{-6}−8.6×10^{-7} cm^2/s at 25 °C, over an order of magnitude less than the direct measured aqueous diffusion coefficient of KBr (2×10^{-5} cm^2/s). Both Cdot and KBr tracers were used without any further purification. Quartz sand provided by AGSCO (Hasbrouck Heights, NJ, USA) was selected as the porous medium. The sand is composed of >98% SiO_2, with minor Al_2O_3, K_2O, and Fe_2O_3. The sand size range is 74−250 μm, and the density is 2.65 g/cm^3. Prior to use, the sand was acid-washed, rinsed in deionized (DI) water, oven-dried, and then resaturated in DI water.[26] The NaCl solution with a concentration of 5000 mg/L was used as the injected brine water.

2.3. Apparatus and Process. As illustrated in Figure 3, fluid was injected at a constant and precise rate using two 60 mL syringes mounted on a continuous-flow syringe pump (780200 V, KD Scientific, Holliston, MA, USA). A peristaltic pump was used to flush the column with brine water of 5000 mg/L NaCl solution. The injection pressure was monitored with a small piezometer filled with water at the model inlet. The effluent was connected to an automatic fraction collector (Foxy R1, Teledyne ISCO, Lincoln, NE, USA), and samples were collected at regular intervals.

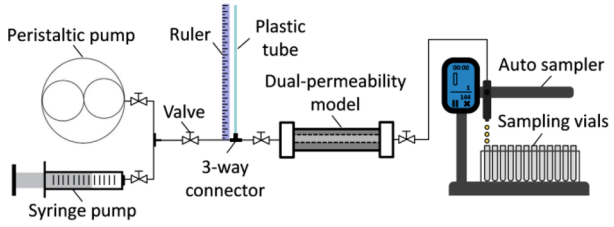

Figure 3. Schematic of experimental setup.

2.4. Methods and Procedures. The quartz sand with different grain size ranges was wet-packed into the central core and annulus of the interior chamber, respectively. Four size ranges of sand were prepared, and they were respectively marked as sand A (74−106 μm), sand B (106−125 μm), sand C (125−177 μm), and sand D (177−250 μm). Prior to column packing, the sand was saturated by immersing in aged DI water and then the container was placed in a vacuum chamber and

DOI: 10.1021/acs.iecr.7b00194
Ind. Eng. Chem. Res. 2017, 56, 7365−7374

Table 1. Basic Parameters for All Columns Used in Our Experiments[a]

column no.	sand type/core/annulus	D_c (cm)	D_t (cm)	V_c (mL)	V_t (mL)	K_c (μm^2)	K_a (μm^2)	$\frac{V_c}{V_t}$	$\frac{K_c}{K_a}$
11#	sand D only	–	1.95	–	20.14	23.87	23.87	–	–
21#	sand D/A	1.04	1.95	5.73	21.43	23.87	3.28	0.27	7.27
31#	sand A/A	1.04	1.95	6.25	21.95	3.28	3.28	0.27	1.00
32#	sand B/A	1.04	1.95	6.14	21.85	9.87	3.28	0.27	3.01
33#	sand C/A	1.04	1.95	5.86	21.56	16.46	3.28	0.27	5.01
34#	sand D/A	1.04	1.95	5.73	21.43	23.87	3.28	0.27	7.27
35#	sand D/–	1.04	1.04	5.73	20.14	23.87	0.00	0.27	∞
41#	sand A/A	0.00	1.95	0.00	21.95	–	3.28	0.00	–
42#	sand D/A	0.50	1.95	1.33	21.83	23.87	3.28	0.06	7.27
43#	sand D/A	1.04	1.95	5.73	21.43	23.87	3.28	0.27	7.27
44#	sand D/A	1.36	1.95	10.09	21.04	23.87	3.28	0.48	7.27
45#	sand D/D	1.95	1.95	20.14	20.14	23.87	–	1.00	–

[a] D_c is the core diameter, D_t is the internal diameter of the column, V_c is the core pore volume, V_t is the total pore volume of the column, K_c is the core permeability, and K_a is the annulus permeability. The core and annulus pore volume and permeability were determined by the porosity and permeability associated with different sand types under the same packing protocol. For sands A, B, C and D, in order, the packing porosity and permeability were 0.42, 3.28 μm^2; 0.41, 9.87 μm^2; 0.39, 16.46 μm^2; and 0.38, 23.87 μm^2. The porosity was measured by the weighing method, and the permeability was measured and calculated according to Darcy's law. The column 35# was constructed from a clear acrylic tube of 1.04 cm inner diameter surrounded by a fictional annulus with the same porosity but zero permeability, and was used to simulate the fractured porous media in this work.

degassed for 30 min. After enough sand was processed carefully, the column together with all its fittings and the copper mesh were immersed in a larger container filled with aged DI water which was then placed in a vacuum chamber and degassed for more than 10 min. When there were no more air bubbles visibly emerging, the bottom fittings were placed on the column keeping all parts submerged. Degassed sand was then slowly deposited into the water-filled column without contact with air. Coarse sand was introduced into the copper mesh with an appropriately sized funnel simultaneously with the introduction of fine sand into the annulus between the copper mesh and inner wall of the acrylic tube. Gentle vibration using two wood blocks was applied uniformly in all directions, and the column was slightly overfilled with sand. Next, the second end fittings were locked onto the overfilled end of the column. The entire packed column, still inside the larger container, was then placed into the vacuum chamber and evacuated overnight. The vacuum pump used in this study was a Vacuubrand ME1 (Germany). Dual tracer test was performed the next day, right after taking the column out of the vacuum chamber. Table 1 lists the basic parameters for all the columns used in our experiments.

Before each experiment, the column was saturated with DI water for 24 h. Then fluids were added in three phases. In phase 1, 4.0 pore volumes (PV) of brine water with a concentration of 5000 mg/L NaCl was injected into the column with a desired flow rate. For phase 2, 4.0 PV of Cdot and KBr mixture in 5000 mg/L NaCl solution was pumped into the column with the same flow rate. In phase 3, the column was flushed with 4.0 PV of brine water with a concentration of 5000 mg/L NaCl at the same flow rate. During phase 2 and phase 3, the effluent samples were collected at a constant regular interval of 2.0 mL. The Cdot concentrations of effluent samples were determined by fluorescence spectrometry using a SpectraMax M2e (Molecular Devices, Sunnyvale, CA, USA). The fluorescent excitation wavelength was 358 nm, and the emission peak at this excitation was 460 nm. The peak emission intensity is a linear function of Cdot concentration below 50 mg/L, and the detection limit is 10 000 mg/L. The KBr concentrations of effluent samples were measured with an ion-selective electrode attached to a handheld pH/mV/temperature meter (6230N, Jenco Instruments, San Diego, CA, USA). Known concentrations of Cdot and KBr standard solutions were used to produce calibration curves prior to each set of experiments. The injection concentrations of Cdot and KBr were 50 mg/L and 1000 mg/L in all experiments. All experiments were conducted at 25 °C. The breakthrough curves (BTCs) were expressed as the relative aqueous concentration (C/C_0) against the number of pore volumes (V/V_t). At the end of phase 2 in each experiment, the relative volume fraction (f, decimal) of the total pore volume of the column filled with tracer (i.e., the fluid displacement or change rate) was calculated using eq 1:

$$f = \frac{\int_0^{t_f} Q\left(1 - \frac{C}{C_0}\right) dt}{V_t} \quad (1)$$

where Q is the injection flow rate, mL/min; C_0 is the injected tracer concentration, mg/L; C is the effluent tracer concentration, mg/L; t_f is the tracer injection duration, min; and V_t is the total pore volume of the column, mL. It is obvious that the f values should never fall lower than the volume fraction represented by the permeable central core. If the injected tracers can fully diffuse into the matrix, the f values should tend to the total pore volume fraction of the column (V_t/V_t).

3. RESULTS AND DISCUSSION

3.1. Conceptual Framework. Actually, the transport mechanisms of tracer in porous media are mainly advection, dispersion, and diffusion.[27] "Advection" refers to the migration process of tracer along with the fluid flow. Advection is the major way for tracer migration in porous media, and increasing the flow rate is related to enhanced advection. "Dispersion" means the chromatographic separation phenomenon of tracer in transverse and longitudinal directions. It could be due to the frictional force between the pore walls and fluids, or caused by the variety of pore size and flow path length. Diffusion is caused by the concentration gradient and random motion, and even if

DOI: 10.1021/acs.iecr.7b00194
Ind. Eng. Chem. Res. 2017, 56, 7365−7374

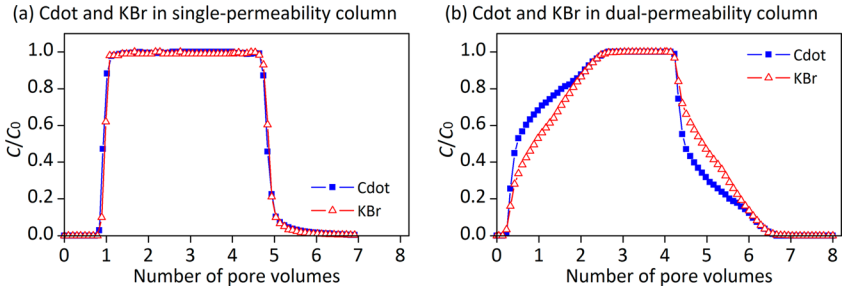

Figure 4. BTCs of Cdot and KBr in (a) single- and (b) dual-permeability columns (11# and 21#) at a flow rate of 0.1 mL/min.

there is no fluid flow, the tracer in solution can diffuse from a zone of greater concentration to one of less concentration.

Considering the transport of tracer in homogeneous porous media, the entire system can be divided into two different but coexistent zones, i.e., the mobile zone and the stagnant zone. In the mobile zone, advection plays an important role in the tracer migration, while diffusion dominates the tracer migration in the stagnant zone. The injected tracer first enters the mobile zone along with the fluid flows, and then part of the tracer diffuses from the mobile zone into the stagnant zone. In fact, the advection in the mobile zone is much faster than the diffusion in the stagnant zone. The tracer traveling through the mobile zone will thus arrive at the outlet earlier, while the tracer diffusing through the stagnant zone will arrive later. In these cases, the tracer in heterogeneous porous media will have a distinct "steplike" arrival curve.

For our dual-permeability columns, there is a high permeable core surrounded by a low permeable matrix. Most of the flow occurs through the high permeable core, but the flow within the low permeable matrix is much more stagnant. If two tracers, one of which is much less diffusive than another, are simultaneously injected into the dual-permeability columns, their BTCs will separate as expected. The less diffusive tracer almost does not diffuse into the stagnant zone, and thus can determine the pore volume of the mobile zone. Besides, the more diffusive tracer can fully diffuse into and fill the stagnant zone, and thus can indicate the total pore volume of the entire column including the mobile zone and the stagnant zone. Therefore, these two tracers can be used to assess the preferential flow in heterogeneous environments. In the next sections, we will consider the breakthrough characteristics of Cdot and KBr tracers in homogeneous and heterogeneous porous media.

3.2. Dual Tracer Breakthrough Characteristics. Observed BTCs of Cdot and KBr in single- and dual-permeability columns (11# and 21#) at a flow rate of 0.10 mL/min are shown in Figure 4. During the injection of Cdot and KBr tracers, both Cdot and KBr were transported mainly through advection in the single-permeability (homogeneous) column (11#). Cdot and KBr arrived at the outlet of the column when the injected pore volume was 0.80 PV (the arrival time, V_a). Then the relative effluent concentration (C/C_0) of Cdot and KBr increased linearly with the continuous injection of them, and at last reached 100% when 1.20 PV of Cdot and KBr tracers was injected (the balance time, V_b), as indicated in Figure 4a. It can also be observed from Figure 4a that there are two transitional zones of pore water and dissolved tracers on BTCs on the left and right sides of 1.00 PV, indicating that the transport of Cdot and KBr tracers in homogeneous porous media has been partly affected by dispersion. Although the Cdot tracer is much less diffusive than the KBr tracer (i.e., a great difference between their aqueous diffusion coefficients), their BTCs almost coincide with each other, as shown in Figure 4a, indicating that diffusion has little influence on the transport of these two tracers in homogeneous porous media.

Comparatively, it can be clearly observed in Figure 4b that the BTCs of Cdot and KBr tracers in the dual-permeability (heterogeneous) column (21#) show different characteristics. When only 0.23 PV of Cdot and KBr tracers (the arrival time, V_a) was injected, both Cdot and KBr arrived at the outlet of the column. However, more volume of Cdot and KBr tracers was needed for their relative effluent concentration (C/C_0) to reach 100%, and the balance time (V_b) was up to about 2.85 PV. Correspondingly, the two transitional zones of pore water and dissolved tracers on both sides of 1.00 PV became even greater. In addition, the BTCs of both Cdot and KBr present a "steplike" arrival behavior as discussed above, and do not coincide with each other. This result indicates that diffusion has great influence on the transport of these two tracers in heterogeneous porous media.

Another important result can be made from the complete experimental mass balance of Cdot and KBr tracers. The relative mass of Cdot and KBr tracers recovered in the effluent (R_m, %) at the end of each experiment can be calculated using eq 2:

$$R_m = \int_0^{t_e} C\ dt/(C_0 t_f) \times 100\% \quad (2)$$

where t_e is the time after the injection of tracers started. As indicated by the BTCs in Figure 4a, 98.70% of Cdot and 99.74% of KBr were recovered in the effluent of the homogeneous porous media. For the heterogeneous porous media, the relative mass of the injected Cdot and KBr recovered in the effluent was up to 97.92 and 99.37%, respectively, as indicated by the BTCs in Figure 4b. The result indicates the Cdot tracer may be retained to a slight degree compared to the KBr tracer. In fact, unwashed sands, natural soils, and reservoir materials are likely to retain some amount of the injected nanoparticles and the retention needs to be considered in field applications, but the results reported here clearly show the diffusion difference of Cdot and KBr tracers into the relatively stagnant matrix and the separation on the BTCs of these two tracers as discussed previously. Because of the little retention of Cdot and KBr tracers in our experiments, we will focus on the BTCs of these two tracers in phase 2 in the following sections.

3.3. Flow Rate Sensitivity Experiments. In order to further investigate the effect of dispersion and diffusion on the transport of Cdot and KBr tracers in heterogeneous porous media, four dual tracer experiments with different flow rates

DOI: 10.1021/acs.iecr.7b00194
Ind. Eng. Chem. Res. 2017, 56, 7365−7374

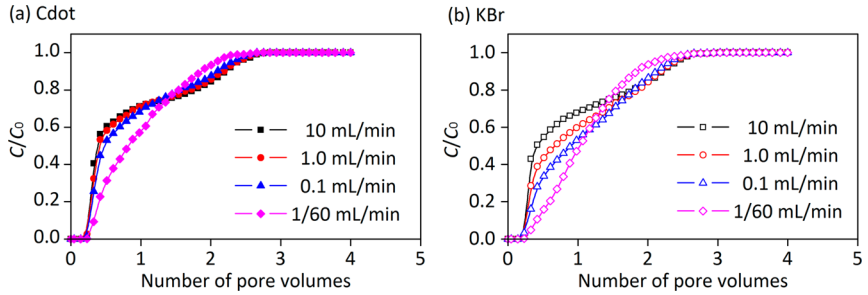

Figure 5. BTCs of (a) Cdot and (b) KBr in dual-permeability column (21#) at different flow rates.

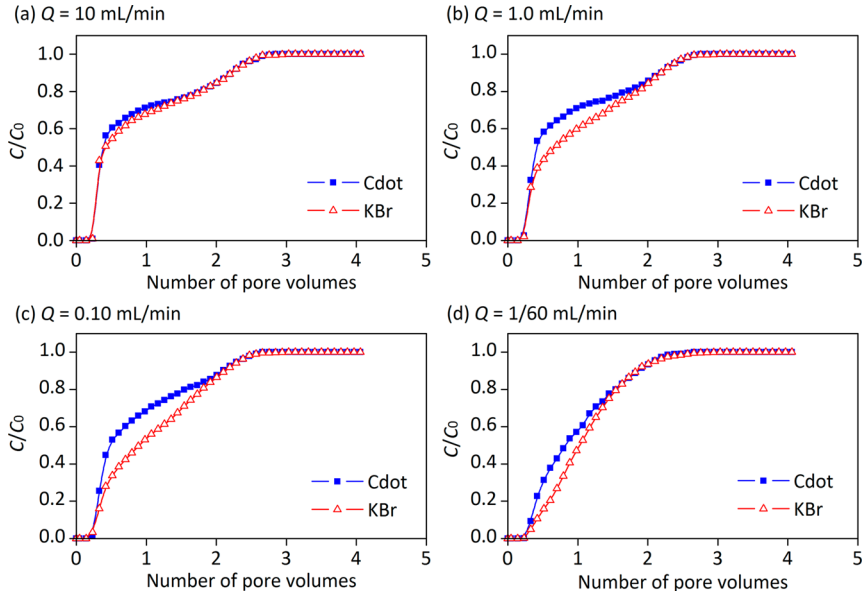

Figure 6. Effect of flow rate (Q) on BTCs of Cdot and KBr in dual-permeability column (21#): (a) Q = 10 mL/min, (b) Q = 1.0 mL/min, (c) Q = 0.1 mL/min, and (d) Q = 1/60 mL/min.

were carried out in this section, and the flow rate (Q) was 1/60, 0.1, 1.0, and 10 mL/min, respectively, which corresponded to true velocity ranging from 0.4 to 250 m/day. The flow rate reflects the injection intensity of Cdot and KBr tracers and the flow states of pore water and dissolved tracers in porous media, and therefore affects the breakthrough characteristics of these two tracers in heterogeneous porous media. Figure 5 shows the BTCs of Cdot and KBr in the dual-permeability column (21#) at different flow rates. It can be seen that the BTCs of Cdot and KBr tracers at different flow rates all present a "steplike" arrival behavior and increasing the flow rate is related to more significant arrival steps.

Additionally, the BTCs of Cdot and KBr at different flow rates do not coincide with each other and there is a closed region between all the BTCs of Cdot and KBr in the dual-permeability column (21#) at different flow rates, as shown in Figure 6. The BTCs of Cdot always locate above the BTCs of KBr, and the size of the closed region first increases and then decreases with the increase of flow rate. Within the four flow rates of this work, the closed region has the largest size when the flow rate is 0.1 mL/min (see Figure 6c). After changing to a large flux of 10 mL/min, the BTCs of both Cdot and KBr present more obvious "steplike" arrival behavior, but nearly coincide with each other (see Figure 6a), indicating that when the flow rate is large, both Cdot and KBr transport mainly through advection in the mobile zone, and their diffusion in the stagnant zone is almost negligible. Furthermore, when reducing the flux to a low level of 1/60 mL/min, the BTCs of Cdot and KBr move toward the bottom right, and at last become two smooth curves without arrival steps (see Figure 6d). In this case, the diffusion of Cdot and KBr in the stagnant zone becomes quite evident as expected. The results show that when the flow rate stays at a low level, the Cdot and KBr tracers will have enough time to diffuse from the mobile zone into the stagnant zone, and thus the arrival time of Cdot and KBr will be delayed.

As discussed above, when the flow rate is excessively large, advection will dominate the migration of the tracer, and thus the tracer does not have enough time to diffuse into the stagnant zone. In this case, the f values calculated using eq 1 will tend to the pore volume ratio of the mobile zone to the entire column (V_m/V_t). Here, V_m is the pore volume of the mobile zone, in milliliters. In contrast, when the flow rate is excessively small, diffusion will dominate the migration of tracer, and the tracer will have enough time to diffuse into the stagnant zone and fully fill the entire column. As a result, the f values will tend to 1.0 (i.e., V_t/V_t), as expected.

On the basis of the BTCs of Cdot and KBr at different flow rates, the f values for Cdot and KBr, i.e., f_{Cdot} and f_{KBr}, were calculated and plotted in Figure 7. It can be seen that when the flow rate is 10 mL/min, the difference between f_{Cdot} and f_{KBr} is extremely small. The value of f_{Cdot} is 0.7444, the value of f_{KBr} is 0.7809, and their difference is only 0.0365. With the decrease of the flow rate, the difference between f_{Cdot} and f_{KBr} first

DOI: 10.1021/acs.iecr.7b00194
Ind. Eng. Chem. Res. 2017, 56, 7365−7374

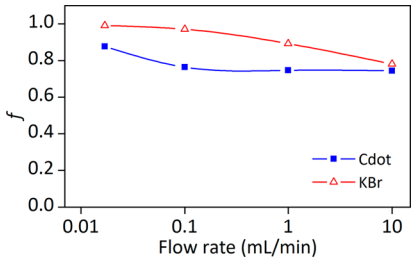

Figure 7. Values of f_{Cdot} and f_{KBr} at different flow rates.

increases and then decreases, as shown in Figure 7. Corresponding to the flow rates of 1.0, 0.1, and 1/60 mL/min, the values of f_{Cdot} are 0.7464, 0.7633, and 0.8726, the values of f_{KBr} are 0.8925, 0.9708, and 0.9904, and their differences are 0.1461, 0.2074, and 0.1218, respectively. When the flow rate is 0.1 mL/min, the difference between f_{Cdot} and f_{KBr} has the biggest value of 0.2074, which corresponds to the largest closed region between the BTCs of Cdot and KBr in Figure 6c.

For the dual chemical−nanoparticle tracer method, the flow rate should be selected and controlled appropriately. As indicated in Figure 7, the values of f_{KBr} all tend to 1.0 and have little difference when the flow rates are 1/60 and 0.1 mL/min, and the values of f_{Cdot} have little difference when the flow rates are 0.1, 1.0, and 10 mL/min. Therefore, the flow rate of 0.1 mL/min will meet the requirement of the dual tracer tests in this work. The less diffusive Cdot tracer can be used to determine the pore volume of the mobile zone ($V_{m\text{-}Cdot}$), and the more diffusive KBr tracer can be used to indicate the pore volume of the entire column ($V_{t\text{-}KBr}$). Thus, these two tracers can be used to assess the preferential flow of heterogeneous environments. Here, the heterogeneity index (H_i) expressed as the ratio of ($f_{KBr} - f_{Cdot}$) to f_{KBr} is introduced to characterize the degree of preferential flow. In the next sections, we will consider the characteristics of Cdot and KBr tracers in different types of heterogeneous porous media.

3.4. Permeability Ratio Sensitivity Experiments. The permeability ratio is an important parameter for evaluating the heterogeneity of heterogeneous environments. In this section, dual tracer experiments were conducted in five columns (31#, 32#, 33#, 34#, and 35#) with different core−annulus permeability ratios (K_c/K_a). The core diameter of all the first four columns was fixed at 1.04 cm. The last experiment was carried out in a sand-packed glass column with an internal diameter of 1.04 cm. In this study, this column was used as a fracture or channel that was surrounded by an imaginary annulus. The annulus porosity was the same as the column, but the annulus permeability was zero. For all five experiments, the flow rate (Q) was kept at 0.1 mL/min. Figure 8 gives the BTCs of Cdot and KBr in the five columns with different core−annulus permeability ratios. Figure 9 shows the effect of core−annulus permeability ratio on the BTCs of Cdot and KBr and the variation curves of the f value versus the core−annulus permeability ratio (K_c/K_a). The characteristics are as follows.

1. For the homogeneous porous media, i.e., when the core−annulus permeability ratio (K_c/K_a) is equal to 1.00, Cdot and KBr transport mainly through advection. The BTCs of Cdot and KBr show the same variation characteristics as discussed in Figure 4a. Due to the influence of dispersion on the migration of tracers in homogeneous porous media is very small, the transitional zones of pore water and dissolved tracers on both sides of 1.00 PV is very small too. Besides, the BTCs of Cdot and KBr almost coincide with each other, and the values of f_{Cdot} and f_{KBr} all tends to 1.0. The value of f_{Cdot} is 0.9805, the value of f_{KBr} is 0.9850, and their difference is only 0.0045. The results also indicate that the diffusion has little influence on the transport of Cdot and KBr in homogeneous porous media.

2. In the heterogeneous porous media, i.e., when the core−annulus permeability ratio (K_c/K_a) is greater than 1.00, Cdot and KBr are mainly transported through advection in the mobile zone, and through diffusion in the stagnant zone. At the same time, the dispersion has a significant impact on the processes of advection and diffusion. With the increase of the permeability ratio (K_c/K_a), less time will be needed by Cdot and KBr to arrival at the outlet of columns, while more time will be used for the relative effluent concentration (C/C_0) to reach 100%, as shown in Figure 8. Besides, the steps on the BTCs move toward the top left, and the transitional zones of pore water and dissolved tracers on both sides of 1.00 PV become larger. More importantly, the separation of Cdot and KBr BTCs occurs, and the closed region between the BTCs of Cdot and KBr is increased as the permeability ratio (K_c/K_a) increases, as indicated in Figure 9b−d. In this case, the values of f_{KBr} all tend to 1.0, while the differences between the values of f_{Cdot} and f_{KBr} become larger and larger, as shown in Figure 9e.

Corresponding to the core−annulus permeability ratios (K_c/K_a) of 3.01, 5.01, and 7.27, the arrival times (V_a) are 0.50, 0.32, and 0.23 PV and the balance times (V_b) are 1.88, 2.46, and 3.22 PV. The values of f_{KBr} are 0.9803, 0.9755, and 0.9708, the values of f_{Cdot} are 0.9428, 0.8635, and 0.7649, and their differences are 0.0375, 0.1120, and 0.2059, respectively. The results indicate that KBr can diffuse rapidly enough into and fully fill the stagnant zone, and Cdot almost cannot diffuse into the stagnant zone. As expected, the size of the stagnant zone in heterogeneous porous media is increased with the increase of the permeability ratio, as indicated by the differences of f_{Cdot} and f_{KBr} values in Figure 9e.

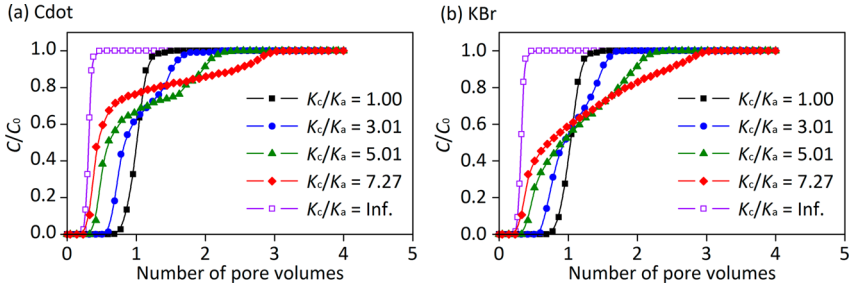

Figure 8. BTCs of (a) Cdot and (b) KBr in dual-permeability columns with different core−annulus permeability ratios (K_c/K_a).

DOI: 10.1021/acs.iecr.7b00194
Ind. Eng. Chem. Res. 2017, 56, 7365−7374

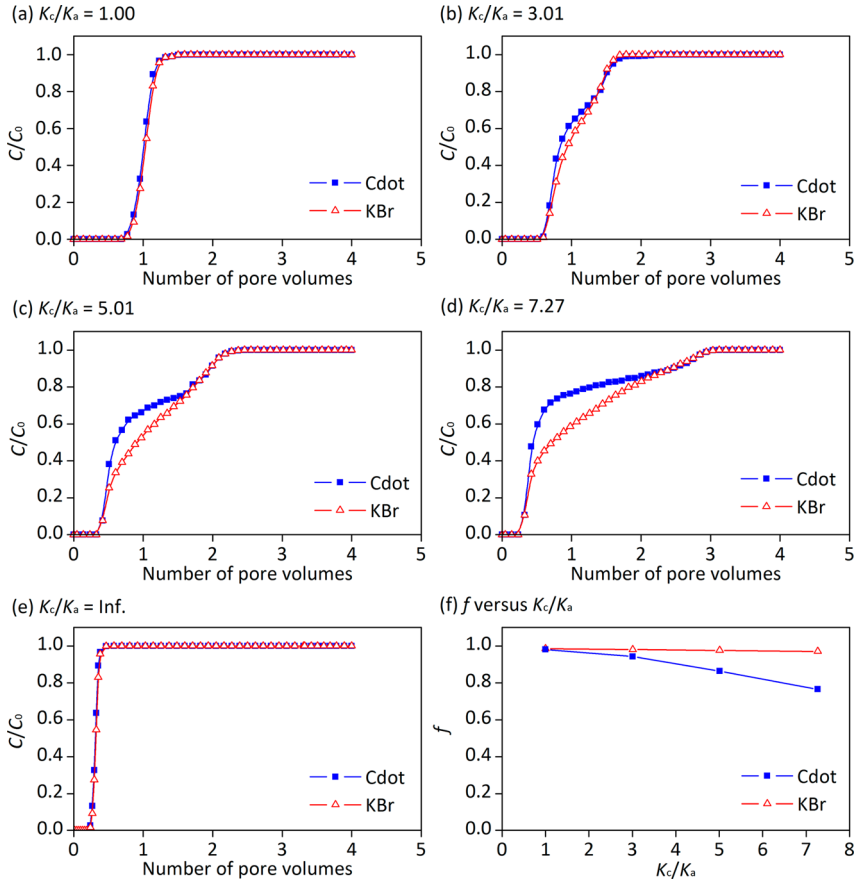

Figure 9. Effect of core−annulus permeability ratio (K_c/K_a) on BTCs of Cdot and KBr: (a) K_c/K_a = 1.00, (b) K_c/K_a = 3.01, (c) K_c/K_a = 5.01, (d) K_c/K_a = 7.27, and (e) K_c/K_a = ∞. (f) Variation curves of f versus K_c/K_a.

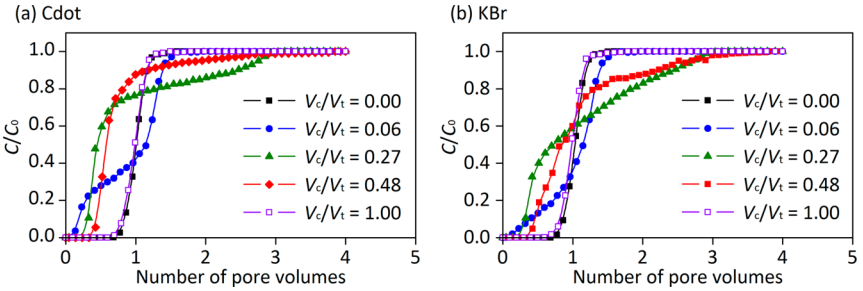

Figure 10. BTCs of (a) Cdot and (b) KBr in dual-permeability columns with different core pore volume ratios (V_c/V_t).

3. For the fractured porous media (the fractures have infinite flow conductivity), i.e., when the core−annulus permeability ratio (K_c/K_a) tends to be infinite, the injected Cdot and KBr traces are only transported in the fractures or channels. The BTCs of Cdot and KBr have similar variation characteristics as discussed in Figure 4a, and the difference is that the transitional zones of pore water and dissolved tracers are located on both sides of 0.28 PV. In this case, the arrival time (V_a) is 0.18 PV, and the balance time (V_b) is 0.38 PV. The BTCs of Cdot and KBr almost coincide with each other, and the values of f_{Cdot} and f_{KBr} all tend to 0.2845. The value of f_{Cdot} is 0.2838, the value of f_{KBr} is 0.2844, and the difference is only 0.0006. The results indicate that, in the low permeability tight porous media, the fractures or channels make it difficult for Cdot and KBr to diffuse into the stagnant zone with extremely low permeability.

4. Based on the values of f_{Cdot} and f_{KBr} at different core−annulus permeability ratios (K_c/K_a) of 1.00, 3.01, 5.01, and 7.27, the values of $V_{m\text{-}Cdot}$ are 21.52, 20.60, 18.62, and 16.39 mL, the values of $V_{t\text{-}KBr}$ are 21.62, 21.42, 21.03, and 20.80 mL, and the heterogeneity indexes (H_i) are 0.0046, 0.0383, 0.1146, and 0.2120, respectively, which indicates that the greater the permeability ratio is, the more prominent the preferential flow will be. Thus, the sweep efficiency of the heterogeneous environments will be low.

3.5. Core Diameter Sensitivity Experiments. For heterogeneous environments, the porosity proportion of fractures or channels is an extremely important factor, which not only affects the reservoir development effect, but also influences the effectiveness of chemical waste and carbon dioxide sequestration. In this section, five columns (41#, 42#, 43#, 44#, and 45#) with various core pore volume ratios (V_c/V_t) were used to carry out the dual tracer experiments. In the first and last experiments, the column (41#) was filled with sand A (74−106 μm) and the column (45#) was packed with sand D

DOI: 10.1021/acs.iecr.7b00194
Ind. Eng. Chem. Res. 2017, 56, 7365−7374

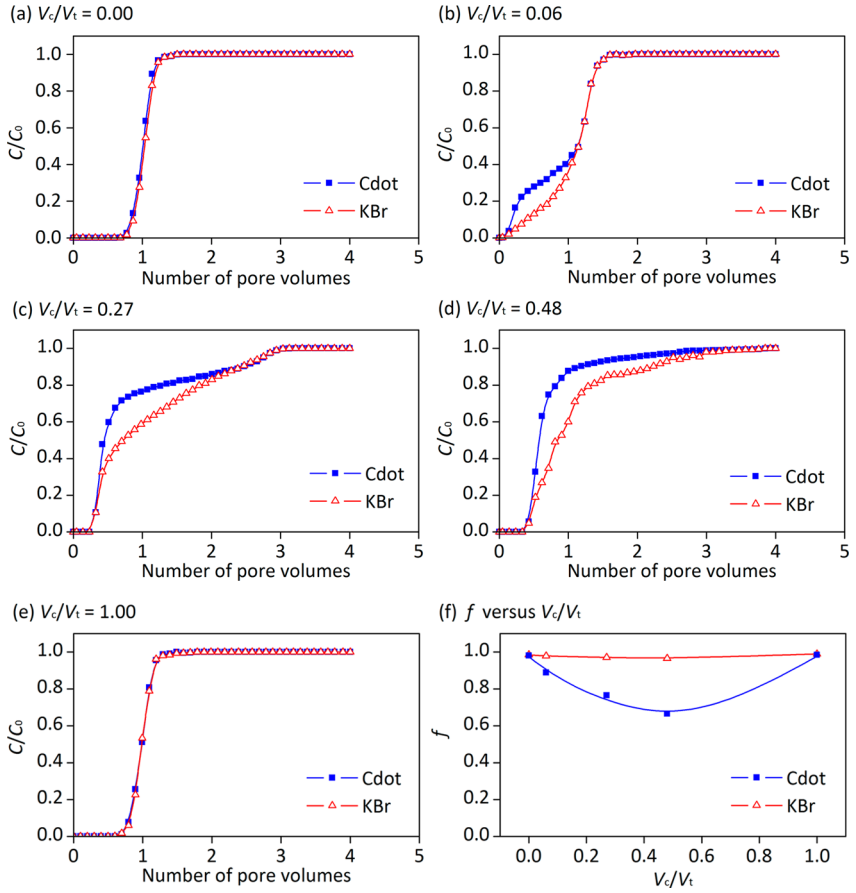

Figure 11. Effect of core pore volume ratio (V_c/V_t) on BTCs of Cdot and KBr: (a) V_c/V_t = 0.00, (b) V_c/V_t = 0.06, (c) V_c/V_t = 0.27, (d) V_c/V_t = 0.48, and (e) V_c/V_t = 1.00. (f) Variation curves of f versus V_c/V_t.

(177−250 μm). In these two columns, there is no core channel. The cores and annuli of the other three columns (42#, 43#, and 44#) were filled with sands D and A, respectively. In this study, the core pore volume ratios (V_c/V_t) of these five columns, in order, were 0.00, 0.06, 0.27, 0.48, and 1.00. For all five experiments, the flow rate (Q) was kept at 0.1 mL/min. Figure 10 gives the BTCs of Cdot and KBr in the five columns with core pore volume ratios. Figure 11 shows the effect of core pore volume ratio on the BTCs of Cdot and KBr and the variation curves of the f value versus the core pore volume ratio (V_c/V_t). The characteristics are as follows.

1. For the homogeneous porous media without high or low permeable zone, i.e., when the core pore volume ratio (V_c/V_t) is 0.00 or 1.00, the BTCs of Cdot and KBr all show the same variation characteristics as discussed in Figure 4a. Corresponding to the core pore volume ratios of 0.00 and 1.00, the arrival time (V_a) is 0.80 PV and the balance time (V_b) is 1.20 PV. The values of f_{Cdot} are 0.9805 and 0.9842, the values of f_{KBr} are 0.9850 and 0.9899, and their differences, in order, are 0.0045 and 0.0057. The results also indicate that diffusion has little influence on the transport of Cdot and KBr in homogeneous porous media.

2. For the heterogeneous porous media with high or low permeable zone, i.e., when the core pore volume ratio (V_c/V_t) is greater than 0.00 and less than 1.00, Cdot and KBr are mainly transported through advection in the mobile zone, and through diffusion in the stagnant zone as discussed above. Nevertheless, the BTCs of Cdot and KBr present different variation characteristics with respect to their BTCs in the heterogeneous columns with different core−annulus permeability ratios (K_c/K_a).

When the core pore volume ratio (V_c/V_t) is less than 0.50, both the arrival time (V_a) and the balance time (V_b) are increased with the increase of core pore volume ratio (V_c/V_t), as shown in Figure 10. In addition, the steps on the BTCs move toward the top right, and the transitional zones of pore water and dissolved tracers on both sides of 1.00 PV become larger and larger. The separation of Cdot and KBr BTCs also occurs, and the size of the closed region between the BTCs of Cdot and KBr is increased as the core pore volume ratio (V_c/V_t) increases, as indicated in Figure 11b−d. As shown in Figure 11e, the values of f_{KBr} tend to 1.0, and the values of f_{Cdot} become smaller and smaller.

Based on the variation trends of the BTCs of Cdot and KBr when the core pore volume ratio (V_c/V_t) is less than 0.50, we can infer that when the core pore volume ratio (V_c/V_t) is greater than 0.50, the transitional zones of pore water and dissolved tracers on both sides of 1.00 PV would become smaller and smaller, and the size of the closed region between the BTCs of Cdot and KBr would be increased as the core pore volume ratio (V_c/V_t) increases. In this case, the values of f_{KBr} would still tend to 1.0, but the values of f_{Cdot} would become larger and larger.

Corresponding to the core pore volume ratios (V_c/V_t) of 0.06, 0.27, and 0.48, the arrival times (V_a) are 0.05, 0.23, and 0.33 PV and the balance times (V_b) are 1.97, 3.22, and 3.94 PV, respectively. The values of f_{KBr} are 0.9785, 0.9708, and 0.9649, the values of f_{Cdot} are 0.8887, 0.7649, and 0.6659, and their

DOI: 10.1021/acs.iecr.7b00194
Ind. Eng. Chem. Res. 2017, 56, 7365−7374

differences are 0.0898, 0.2059, and 0.2990, respectively. These results also indicate that KBr can diffuse rapidly enough into and fully fill the stagnant zone, whereas Cdot almost cannot diffuse into the stagnant zone.

3. Based on the values of f_{Cdot} and f_{KBr} at different core pore volume ratios (V_c/V_t) of 0.00, 0.06, 0.27, 0.48, and 1.00, the values of $V_{m\text{-}Cdot}$ are 21.52, 19.40, 16.39, 14.01, and 19.82 mL, the values of $V_{t\text{-}KBr}$ are 21.62, 21.36, 20.80, 20.30, and 19.94 mL, and the heterogeneity indexes (H_i) are 0.0046, 0.0918, 0.2120, 0.3099, and 0.0060, respectively. When the core pore volume ratio (V_c/V_t) is 0.50, the preferential flow would be more prominent, and the sweep efficiency of the heterogeneous environments would be worse.

3.6. Essential Characteristics of Dual Tracer Tests. As indicated by the BTCs of Cdot and KBr tracers in homogeneous and heterogeneous porous media, the essential characteristics of dual KBr−Cdot tracer tests are as follows:

1. If the BTCs of Cdot and KBr tracers coincide with each other, and their f values are both approximately equal to 1.0, this indicates a relatively homogeneous environment without high or low permeable zones.

2. If the BTCs of Cdot and KBr tracers coincide with each other, but their f values are both significantly less than 1.0, this indicates a heterogeneous environment with fractures or channels surrounded by an extremely low permeable matrix.

3. If the BTCs of Cdot and KBr tracers separate, and both have obvious "steplike" variation characteristics, this indicates a heterogeneous environment with high and low permeable zones.

4. If the steps on the BTCs of Cdot and KBr tracers move toward the top left, the arrival time (V_a) is decreased, and the balance time (V_b) is increased, this means that the permeability ratio of the heterogeneous environments becomes greater.

5. If the steps on the BTCs of Cdot and KBr tracers move toward the top right and the arrival time (V_a) and the balance time (V_b) are both increased, this means that the high permeable zone (or the low permeable zone) in the heterogeneous environments becomes larger.

6. When the value of f_{KBr} is approximately equal to 1.0, if the value of f_{Cdot} is close to 1.0, i.e., the heterogeneity index (H_i) tends to 1.0, this means that the preferential flow is not significant and the sweep efficiency of the heterogeneous environments is better. The smaller the value of f_{Cdot} is, the more prominent the preferential flow will be, and the sweep efficiency will become worse.

As discussed with previous dual tracer experiments in saturated homogeneous and heterogeneous columns, nanoparticles together with a chemical tracer can assess the preferential flow. With the injection rate selected and controlled appropriately, the inert carbon nanoparticles can be used to implement the dual tracer tests in heterogeneous environments.

4. CONCLUSIONS

In this work, a saturated dual-permeability model with a high permeable core channel surrounded by a low permeable annulus was constructed and used to determine the viability of an inert carbon nanoparticle tracer for the assessment of preferential flow. A series of column experiments were conducted to implement the dual tracer tests in heterogeneous environments by simultaneously injecting chemical and nanoparticle tracers. The major conclusions are as follows:

1. With an appropriate injection rate, the more diffusive KBr tracer can diffuse rapidly enough into the stagnant zone and thus indicate the total pore volume of the system. In contrast, the less diffusive Cdot tracer can almost not diffuse into the stagnant zone, and thus determine the pore volume of the mobile zone. Therefore, they can be used to indicate the preferential flow of heterogeneous environments.

2. The BTCs of Cdot and KBr tracers are almost coincident with each other under homogeneous conditions, but will separate and present obvious "steplike" variation characteristics under heterogeneous conditions. The greater the permeability ratio of heterogeneous environments is, the more prominent the preferential flow will be. The core pore volume ratio also has an important influence on the degree of preferential flow of the heterogeneous environments.

3. The Cdot tracer is likely to be retained to a slight degree compared to the KBr tracer, especially in real heterogeneous environments with unwashed sands, natural soils, or reservoir materials, but the results in our experiments clearly show the diffusion difference of Cdot and KBr tracers into the relatively stagnant matrix and the separation on the BTCs of these two tracers. For the future, the retention of the injected nanoparticles needs to be considered in field applications.

AUTHOR INFORMATION

Corresponding Authors

*E-mail: cy375@upc.edu.cn (C.Y.).
*E-mail: lmc19@cornell.edu (L.M.C.).

ORCID

Chuanjin Yao: 0000-0002-6125-8991
Guanglun Lei: 0000-0002-8209-8974

Author Contributions

#C. Yao and Y. Zhao contributed equally to this work and share first authorship.

Notes

The authors declare no competing financial interest.

ACKNOWLEDGMENTS

We thank experts in the Cornell University Department of Biological and Environmental Engineering for advice and materials, and the Cornell University Physics Department Machine Shop for fabrication of the apparatus. This research was supported by Award KUS-C1-018-02, made by King Abdullah University of Science and Technology (KAUST), the general fund contribution to L. M. Cathles from the International Research Institute of Stavanger, the National Natural Science Foundation of China (Grant 51604291), the Natural Science Foundation of Shandong Province (Grant ZR2016EEB05), the Applied Fundamental Research Project Funded by Original Innovation Program of Qingdao City (Grant 17-1-1-34-jch), the Fundamental Research Funds for the Central Universities (Grants 17CX02010A, 15CX08004A), the China Scholarship Council for C. Yao (Grant 201306450015), and the Program for Changjiang Scholars and Innovative Research Team in University (IRT1294).

REFERENCES

(1) Parkhurst, D. L.; Appelo, C. A. J. *User's Guide to PHREEQC (Version 2): A Computer Program for Speciation, Batch-Reaction, One-Dimensional Transport, and Inverse Geochemical Calculations*; U.S. Geological Survey: Denver, CO, USA, 1999.

(2) Steenhuis, T. S.; Baver, C. E.; Hasanpour, B.; Stoof, C. R.; DiCarlo, D. A.; Selker, J. S. Pore scale consideration in unstable gravity driven finger flow. *Water Resour. Res.* **2013**, *49*, 7815−7819.

DOI: 10.1021/acs.iecr.7b00194
Ind. Eng. Chem. Res. 2017, 56, 7365−7374

(3) Becker, M. W.; Shapiro, A. M. Tracer transport in fractured crystalline rock: Evidence of nondiffusive breakthrough tailing. *Water Resour. Res.* **2000**, *36*, 1677−1686.
(4) Berlin, J. M.; Yu, J.; Lu, W.; Walsh, E. E.; Zhang, L.; Zhang, P.; Chen, W.; Kan, A. T.; Wong, M. S.; Tomson, M. B.; Tour, J. M. Engineered nanoparticles for hydrocarbon detection in oil-field rocks. Energy Environ. *Energy Environ. Sci.* **2011**, *4*, 505−509.
(5) Yao, C. J.; Lei, G. L.; Cathles, L. M.; Steenhuis, T. S. Pore-scale investigation of micron-size polyacrylamide elastic microspheres (MPEMs) transport and retention in saturated porous media. *Environ. Sci. Technol.* **2014**, *48*, 5329−5335.
(6) Xu, Y. S.; Chen, L.; Zhao, Y. S.; Cathles, L. M.; Ober, C. K. Supercritical CO_2-philic nanoparticles suitable for determining the viability of carbon sequestration in shale. *Environ. Sci.: Nano* **2015**, *2*, 288−296.
(7) Cheraghian, G.; Hemmati, M.; Masihi, M.; Bazgir, S. An experimental investigation of the enhanced oil recovery and improved performance of drilling fluids using titanium dioxide and fumed silica nanoparticles. *J. Nanostruct. Chem.* **2013**, *3*, 78.
(8) Pruess, K. On CO_2 fluid flow and heat transfer behavior in the subsurface, following leakage from a geologic storage reservoir. *Environ. Geol.* **2008**, *54*, 1677−1686.
(9) Juanes, R.; Spiteri, E. J.; Orr, F. M.; Blunt, M. J. Impact of relative permeability hysteresis on geological CO_2 storage. *Water Resour. Res.* **2006**, *42*, W12418.
(10) Subramanian, S. K.; Li, Y.; Cathles, L. M. Assessing preferential flow by simultaneously injecting nanoparticle and chemical tracers. *Water Resour. Res.* **2013**, *49*, 29−42.
(11) Li, Y. V.; Cathles, L. M.; Archer, L. A. Nanoparticle tracers in calcium carbonate porous media. *J. Nanopart. Res.* **2014**, *16*, 2541.
(12) Serres-Piole, C.; Preud'homme, H.; Moradi-Tehrani, N.; Allanic, C.; Jullia, H.; Lobinski, R. Water tracers in oilfield applications: Guidelines. J. Petrol. *J. Pet. Sci. Eng.* **2012**, *98*−*99*, 22−39.
(13) Li, Y. V.; Cathles, L. M. The surface interactions of a near-neutral carbon nanoparticle tracer with calcite. *J. Nanopart. Res.* **2016**, *18*, 71.
(14) Bradford, S. A.; Bettahar, M.; Simunek, J.; Van Genuchten, M. T. Transport and fate of colloids in physically heterogeneous porous media. *Vadose Zone J.* **2004**, *3*, 384−394.
(15) Niehren, S.; Kinzelbach, W. Artificial colloid tracer tests: Development of a compact on-line microsphere counter and application to soil column experiments. *J. Contam. Hydrol.* **1998**, *35*, 249−259.
(16) Newman, J. S.; Thomas-Alyea, K. E. *Electrochemical Systems*; John Wiley & Sons, Inc.: Hoboken, NJ, USA, 2004.
(17) Savage, N.; Diallo, M. S. Nanomaterials and water purification: Opportunities and challenges. *J. Nanopart. Res.* **2005**, *7*, 331−342.
(18) Li, M.; Wang, C. W.; O'Connell, M. J.; Chan, C. K. Carbon nanosphere adsorbents for removal of arsenate and selenate from water. *Environ. Sci.: Nano* **2015**, *2*, 245−250.
(19) Yao, C. J.; Lei, G. L.; Li, L.; Gao, X. M. Selectivity of pore-scale elastic microspheres as a novel profile control and oil displacement agent. *Energy Fuels* **2012**, *26*, 5092−5101.
(20) Sang, Q.; Li, Y. J.; Yu, L.; Li, Z. Q.; Dong, M. Z. Enhanced oil recovery by branched-preformed particle gel injection in parallel-sandpack models. *Fuel* **2014**, *136*, 295−306.
(21) Wang, B.; Lin, M. Q.; Guo, J. R.; Wang, D. L.; Xu, F. Q.; Li, M. Y. Plugging properties and profile control effects of cross-linked polyacrylamide microspheres. *J. Appl. Polym. Sci.* **2016**, *133*, 43666.
(22) Li, Z. M.; Sun, M. S.; Lin, R. Y.; Li, Y.; Xu, Y. H. Laboratory study on foam plugging and selective divided-flow. *Acta Petrol. Sin.* **2007**, *28*, 115−118.
(23) Saiers, J. E.; Hornberger, G. M.; Harvey, C. Colloidal silica transport through structured, heterogeneous porous media. *J. Hydrol.* **1994**, *163*, 271−288.
(24) Krysmann, M. J.; Kelarakis, A.; Dallas, P.; Giannelis, E. P. Formation mechanism of carbogenic nanoparticles with dual photoluminescence emission. *J. Am. Chem. Soc.* **2012**, *134*, 747−750.
(25) Markova, Z.; Bourlinos, A. B.; Safarova, K.; Polakova, K.; Tucek, J.; Medrik, I.; Zboril, R.; Siskova, K.; Petr, J.; Krysmann, M.; Giannelis, E. P. Synthesis and properties of core-shell fluorescent hybrids with distinct morphologies based on carbon dots. *J. Mater. Chem.* **2012**, *22*, 16219−16223.
(26) Zevi, Y.; Dathe, A.; McCarthy, J. F.; Richards, B. K.; Steenhuis, T. S. Distribution of colloid particles onto interfaces in partially saturated sand. *Environ. Sci. Technol.* **2005**, *39*, 7055−7064.
(27) Bedient, P. B.; Rifa, H. S.; Newell, C. J. *Ground Water Contamination: Transport and Remediation*; Prentice Hall: Upper Saddle River,NJ, USA, 1999.

DOI: 10.1021/acs.iecr.7b00194
Ind. Eng. Chem. Res. 2017, 56, 7365−7374